Phys. Status Solidi B **250**, No. 5, 957–967 (2013) / **DOI** 10.1002/pssb.201248520

Disorder in Order:
A special issue on amorphous materials
honoring S. R. Elliott

physica status solidi b
www.pss-b.com
basic solid state physics

Editor's Choice

High-density remote plasma sputtering of high-dielectric-constant amorphous hafnium oxide films

Flora M. Li[1], Bernhard C. Bayer[1], Stephan Hofmann[1], Stuart P. Speakman[1], Caterina Ducati[2], William I. Milne[1,3], and Andrew J. Flewitt[*,1]

[1] Electrical Engineering Division, Engineering Department, Cambridge University, J J Thomson Avenue, Cambridge CB3 0FA, UK
[2] Department of Materials Science and Metallurgy, Cambridge University, Pembroke Street, Cambridge CB2 3QZ, UK
[3] Kyung Hee University, Display Research Laboratory, Department of Information Display, Seoul 130701, South Korea

Received 1 November 2012, revised 4 January 2013, accepted 25 January 2013
Published online 7 March 2013

Keywords amorphous materials, hafnium oxide, high-*k* dielectrics, thin film transistors

* Corresponding author: e-mail ajf@eng.cam.ac.uk, Phone: +44 1223 748332, Fax: +44 1223 748348

Hafnium oxide (HfO_x) is a high dielectric constant (k) oxide which has been identified as being suitable for use as the gate dielectric in thin film transistors (TFTs). Amorphous materials are preferred for a gate dielectric, but it has been an ongoing challenge to produce amorphous HfO_x while maintaining a high dielectric constant. A technique called high target utilization sputtering (HiTUS) is demonstrated to be capable of depositing high-k amorphous HfO_x thin films at room temperature. The plasma is generated in a remote chamber, allowing higher rate deposition of films with minimal ion damage. Compared to a conventional sputtering system, the HiTUS technique allows finer control of the thin film microstructure. Using a conventional reactive rf magnetron sputtering technique, monoclinic nanocrystalline HfO_x thin films have been deposited at a rate of $\sim$1.6 nm min^{-1} at room temperature, with a resistivity of 10^{13} Ω cm, a breakdown strength of 3.5 MV cm^{-1} and a dielectric constant of $\sim$18.2. By comparison, using the HiTUS process, amorphous HfO_x ($x = 2.1$) thin films which appear to have a cubic-like short-range order have been deposited at a high deposition rate of $\sim$25 nm min^{-1} with a high resistivity of 10^{14} Ω cm, a breakdown strength of 3 MV cm^{-1} and a high dielectric constant of $\sim$30. Two key conditions must be satisfied in the HiTUS system for high-k HfO_x to be produced. Firstly, the correct oxygen flow rate is required for a given sputtering rate from the metallic target. Secondly, there must be an absence of energetic oxygen ion bombardment to maintain an amorphous microstructure and a high flux of medium energy species emitted from the metallic sputtering target to induce a cubic-like short range order. This HfO_x is very attractive as a dielectric material for large-area electronic applications on flexible substrates.

© 2013 WILEY-VCH Verlag GmbH & Co. KGaA, Weinheim

1 Introduction Hafnium oxide (HfO_x) is a wide bandgap material whose high resistivity, high dielectric constant, k, and large conduction and valence band offset with respect to silicon has led to its adoption as a replacement for silicon dioxide as the gate dielectric in CMOS devices [1, 2]. In particular, the high value of k (typically $\sim$25) allows the thickness of the gate insulator to be increased whilst maintaining the same gate capacitance, resulting in a reduction in the gate leakage current due to electron tunnelling [3–5]. The industrial relevance of HfO_2 is evident by Intel Corporation's milestone of incorporating high-k hafnium-based dielectric material into their 45-nm CMOS process technology [6, 7]. Thin film transistors (TFTs) based on metal oxide channel materials such as zinc oxide (ZnO), [8–14] indium zinc oxide (IZO) [15, 16] and indium gallium zinc oxide (IGZO) [17–19] may equally benefit from incorporation of HfO_2 as the gate dielectric. The motivation for this is the drive towards flexible displays on plastic substrates using organic (polymer or small molecule) light emitting diodes (OLEDs) [20]. In a similar fashion to the commonly available active matrix (AM) liquid crystal displays (LCDs), OLED displays also require an AM array of TFTs to control the light emission from each pixel. However, the performance required of the TFTs is quite

© 2013 WILEY-VCH Verlag GmbH & Co. KGaA, Weinheim

different and, in particular, the TFTs in AMOLED displays require a much higher on-state current and greater duty cycle compared to those used for AMLCDs.

The TFTs that are currently used in AMLCDs are based upon an hydrogenated amorphous silicon (a-Si:H) channel and silicon nitride (SiN_x) gate insulator. They suffer from a significant threshold voltage shift as a function of time with a gate bias applied, and deposition by standard rf plasma enhanced chemical vapor deposition (PECVD) typically requires the substrate to be heated to temperatures in excess of 200 °C, which is incompatible with most plastic substrates [21]. Although other techniques are being developed to allow deposition at lower temperatures [22–26] and compensation circuits are being devised to counteract the threshold voltage shift [27, 28] to allow a-Si:H TFTs to be used in AMOLED displays, both of these approaches add complexity to the device fabrication process. Compared to the incumbent a-Si:H TFT technology, metal oxide TFTs have demonstrated a much higher field effect mobility (typically 10–50 $cm^2 V^{-1} s^{-1}$) and enhanced stability, making them an attractive alternative for AMOLED display backplane applications.

Although much has been made of the selection of the metal oxide semiconductor in published literature for metal oxide TFTs, there has been less focus on the equally important choice of gate dielectric. HfO_x is one such candidate material. Deposition of HfO_x has been achieved using pulsed laser deposition (PLD) [29], atomic layer deposition (ALD) from metalorganic precursors [2, 30], and rf magnetron sputtering from a HfO_2 target [31, 32] and a metallic Hf target [33, 34] in a gas mixture of argon and oxygen. However, in order to achieve good electrical characteristics, deposition at high temperatures or a post-deposition anneal is required. In addition, PLD and ALD operate at relatively low growth rates of 0.1–1 nm min^{-1}. This limits the potential process scalability for high volume manufacturing on an industrial scale where films of tens to hundreds of nanometres in thickness are required, especially for thin film electronic application such as TFT arrays for display backplanes.

Amongst the various deposition techniques, ALD has been the most frequently studied for depositing the HfO_2 gate dielectric for CMOS devices at elevated temperatures. The resulting HfO_2 films tend to be polycrystalline, and may consist of various crystalline phases: monoclinic, cubic, tetragonal, and orthorhombic [1, 3–5, 35, 36]. The monoclinic phase is the most stable polymorph of HfO_2 under normal conditions (i.e., the most stable phase for HfO_2), but it has the lowest k value (∼20). The cubic phase, which is metastable, but can exist indefinitely under normal conditions, has a higher k (∼30) whilst the tetragonal phase has the highest k value (∼40 or higher) [36, 37]. While polycrystalline HfO_2 may contain phases with higher k values at local sites, the presence of grains and grain boundaries in polycrystalline films has an undesirable influence on the device-to-device uniformity, leakage current and device stability. Therefore, amorphous gate dielectrics are preferable. However, it has remained an ongoing challenge to deposit amorphous HfO_2 at low temperature with high k values (>20).

The authors have previously reported that a high-k ($k \sim 30$) cubic-like amorphous HfO_x (*ca*-HfO_x, $x = 2.1$) phase exists in thin film form [38]. The present paper discusses the mechanism by which this *ca*-HfO_x may be deposited at low temperature using a technique called high target utilization sputtering (HiTUS). The advantages of the HiTUS technique are illustrated by comparing HfO_x films

Flora Li is Senior Scientist at Holst Centre/TNO, involved in the development of barrier and electrodes for OLED/OPV devices and R&D in flexible OLED displays. She is also the Project Manager for a European Commission FP7 Project called Flex-o-Fab, which is aimed towards developing a pre-pilot manufacturing route for flexible OLED foils. Before joining Holst Centre, she worked at Polymer Vision as a Senior Scientist and Project Leader on the development of low-temperature oxide TFT backplanes for integration in rollable OLED and e-paper displays. She was a post-doctoral fellow at the University of Cambridge, UK, with a research focus on transparent metal oxide materials and thin film devices. She received the Ph.D. degree in Electrical and Computer Engineering from the University of Waterloo, Canada, in 2008, where she investigated the integration of organic thin film transistors. Dr. Li is a co-author of 20+ refereed publications and two books: CCD Image Sensors in Deep-Ultraviolet (Springer, 2005) and Organic Thin Film Transistor Integration: A Hybrid Approach (John Wiley & Sons, 2011).

Andrew J. Flewitt received the B.Sc. degree in physics from the University of Birmingham, Birmingham, U.K., in 1994 and the Ph.D. degree in scanning tunneling microscopy of amorphous silicon from the University of Cambridge, Cambridge, U.K., in 1998. Following this, he was a Research Associate studying the low-temperature growth of silicon-based materials in the Engineering Department, University of Cambridge. He was appointed to a Lectureship in the same Department in 2002. Since 2009, he has held the position of University Reader in Electronic Engineering. His research interests span a broad range of large area electronics and related fields, including thin film transistors and MEMS devices. Dr. Flewitt is a Chartered Physicist and a Member of the Institute of Physics and the Institution of Engineering and Technology.

© 2013 WILEY-VCH Verlag GmbH & Co. KGaA, Weinheim

deposited by this method with those deposited by conventional 13.56 MHz radio-frequency (rf) magnetron sputtering. No intentional substrate heating and no post-deposition annealing is employed in either case, resulting in a process that is compatible with the use of plastic substrates. Reactive sputtering from a metallic target in the presence of argon and oxygen gases is used in both techniques. It is demonstrated that the use of a metallic target affords control of the oxidation state of the surface of the target and sample.

An optimization study of HfO_x thin films deposited by rf magnetron sputtering and HiTUS is described in the following sections. The electrical and physical properties of the optimized material is presented and correlated with the energetics of deposition. The material properties are compared with the requirements of a gate dielectric in TFT applications.

2 Experimental

2.1 Rf magnetron sputtering

A standard rf magnetron sputtering system (CCR Technology GmbH) was used for HfO_x deposition. The system contains three targets. The vacuum chamber is pumped by a turbo/rotary pump combination and a base pressure of $\sim 10^{-6}$ mbar is achieved prior to deposition. 13.56 MHz rf radiation is applied to a 100 mm diameter metallic hafnium target of 99.999% purity (Testbourne Ltd.) in an atmosphere of argon and oxygen gases, both of which have a 99.999% purity (BOC Gases Ltd). Gas flow is regulated by mass flow controllers. A stainless steel shroud is placed around the target that extends down to just above the sample, which is 100 mm below the target. The shroud is only used for metallic oxide depositions, and therefore serves to reduce the contamination of the sputtered HfO_x sample by other impurities in the vacuum chamber. Furthermore, it confines the plasma to a small volume, thereby increasing the deposition rate for a given rf power.

2.2 High target utilization sputtering (HiTUS)

A schematic diagram of the HiTUS deposition system is illustrated in an earlier publication [39]. The HiTUS deposition system generates a remote, high-density rf argon plasma in the sidearm, which is then amplified and directed onto the target using two electromagnets. Although the plasma has a high density $\sim 10^{13}\,cm^{-3}$, the ion energy is <50 eV, and hence sputtering is only achieved with the application of an additional target bias. This enables a high level of independent control of the sputter deposition parameters and decouples the ion density (which is controlled by the rf antenna power supply) from the ion energy (which is controlled by the bias power supply). The substrate to target distance is 250 mm, and so the sample is removed from the magnetically confined sputtering plasma. A reactive deposition process is used to generate the oxide film required. This is when a metal target is used with an argon/oxygen gas mixture resulting in very high deposition rates. The argon and oxygen are injected into the chamber separately using gas distribution rings, with the argon next to the target and the oxygen in close proximity to the substrate. The remote generation of the plasma enables nearly full target erosion; this substantially reduces the level of target poisoning observed compared to magnetron processes [40], and no feedback mechanism is required. Deposition of HfO_x is performed using the HiTUS system without intentional substrate heating from a 4″ diameter metallic hafnium target of 99.999% purity and 6 mm thickness (Testbourne Ltd) in an atmosphere of argon and oxygen gases, both of which have a 99.999% purity (BOC Gases Ltd). The chamber is pumped to a base pressure of 2×10^{-6} mbar. Argon gas is then admitted at a flow of 50 sccm which raises the pressure to 2×10^{-3} mbar. The rf launch power is 1 kW, the DC bias power is varied from 600 to 1200 W, and the oxygen flow is varied between 10 and 20 sccm.

2.3 Characterization methods

HfO_x samples, with film thickness in the range of 50–300 nm, were deposited onto clean, n-type Si(100) wafers. Their refractive index and thickness were determined using a Gaertner He–Ne (633 nm) ellipsometer. The thickness of selected films was cross-checked by cross-sectional transmission electron microscopy (TEM) and X-ray photoelectron spectroscopy (XPS) depth profiling using Ar-ion sputtering.

Metal-insulator-semiconductor (MIS) capacitor structures were formed by thermally evaporating chromium/aluminum bilayer contacts of ~ 100 nm thickness onto the HfO_x sample through a shadow mask with holes of 0.5, 0.7, and 1.0 mm diameter. Electrical characterization was performed using an Agilent B1500A Semiconductor Parameter Analyser or a Hewlett Packard HP4140B picoammeter/voltage source, and a Hewlett Packard HP4192A LF impedance analyzer. A delay time of several seconds was used between the application of a voltage and measurement of the current to allow the reading to stabilize. The resistivity was calculated from current–voltage (I–V) measurements at an applied field strength of $1\,MV\,cm^{-1}$, as this is a typical operating field in a TFT. The breakdown field was defined to have occurred when the current density reached $0.02\,A\,m^{-2}$ [41]. The dielectric constant was extracted from capacitance–voltage (C–V) characteristics, measured at a frequency between 1 kHz and 1 MHz, using the formula

$$C = \frac{k\varepsilon_0 A}{d}, \quad (1)$$

where C is the measured capacitance, ε_0 is the permittivity of free space, A the capacitor area, and d is the film thickness.

Samples for plan view TEM were deposited onto silicon nitride membranes and analyzed using a Tecnai F20 instrument operating at 200 kV. X-ray diffraction (XRD) measurements (theta–theta scans) were performed using a Bruker D8 with Cu Kα (0.154 nm) radiation. Samples were tilted out of plane by 3° to supress the intense (400) reflection of the single-crystalline Si wafer. The experimental diffrac-

© 2013 WILEY-VCH Verlag GmbH & Co. KGaA, Weinheim

tion patterns were matched with reference patterns from the International Centre for Diffraction Data (ICDD; powder diffraction files 53–0550 and 34–0104) and with [35]. XPS was performed using an Amicus Photoelectron Spectrometer. The optical transmission spectrum was measured using a Perkin Elmer LAMBDA 950 UV/Vis/NIR Spectrophotometer.

3 Results and discussion

3.1 Rf magnetron sputtered films Rf magnetron sputtering of HfO_x takes place at gas pressures $\sim 1 \times 10^{-3}$ mbar. At this pressure, the mean free path of species in an O_2/Ar gas mixture is 5.5 cm, and this is relatively independent of the gas mixture due to the very similar collision diameter of these two gases [42]. Therefore, it is clear that the likelihood of gas phase reactions between Hf atoms that have been sputtered from the target and oxygen species in the plasma is very low. On the other hand, Hf is one of the most easily oxidized metals – indeed, it is often used as a getter for oxygen gas. The time for complete exposure of a surface to a gas at a pressure of $\sim 10^{-3}$ mbar is $\sim 10^{-3}$ s. It follows that this is also a good measure of the time required to oxidize the Hf target surface. Hence, the mechanism by which HfO_x is sputtered from a metallic target is a two-stage process: firstly the target surface is oxidized and subsequently HfO_x species are sputtered from the target, primarily by the high mass argon ions in the plasma. The observation of a colored HfO_x thin film on the target surface at the end of a deposition is indicative of this oxidation process.

High quality HfO_x is deposited under conditions where the oxidation rate is sufficiently high relative to the sputtering rate to ensure that metallic Hf is not sputtered. Under low pressure conditions, an optimum flow ratio of O_2/Ar is observed. This can be seen in the variation in refractive index and deposition rate as a function of flow ratio shown in Fig. 1. For low O_2/Ar flow ratios, there is insufficient oxygen present for oxidation of the Hf target surface, whilst the high concentration of Ar means that the sputtering rate (and hence the deposition rate) is high. For very high O_2/Ar ratios, there is insufficient Ar present to maintain an effective sputtering process as the target becomes heavily poisoned, and the deposition rate falls appreciably, as does the refractive index. Based on Fig. 1, the optimal O_2/Ar flow ratio for the rf magnetron sputtering system is near 1:1. This is higher than might be expected due to the presence of the shroud which limits the ingress of gas into the plasma region, where the oxygen is effectively consumed in the oxidation process. The optimum flow ratio is reduced when no target shroud is employed.

Figure 2 shows how the current density varies as a function of applied electric field for an optimized HfO_x sample (based on an O_2/Ar flow ratio of 1:1). Very low current densities are observed under the application of moderate electric fields which corresponds to a resistivity of $(3.8 \pm 0.3) \times 10^{13}\,\Omega$ cm. This is comparable with the resistivity of silicon nitride used in a-Si:H TFTs. Under these moderate electric fields (~ 1 MV cm^{-1}), Poole-Frenkel conduction dominates, as can be seen by the linear form of the graph shown as the inset to Fig. 2. The Poole-Frenkel current is governed by the relation

$$J = E \exp\left(\frac{2a\sqrt{E} - b\phi_b}{k_B T}\right), \tag{2}$$

where J is the current density, E the electric field strength, ϕ_b the barrier height, k_B the Boltzmann constant, T the absolute temperature, and a and b are constants. Such conduction is caused by the excitation of trapped electrons into the conduction band of the insulator where the field reduces the barrier [43]. The material is found to break down under the application of an electric field of 3.5 MV cm^{-1} for a sample of ~ 100 nm thickness.

The capacitance–voltage curves for MIS structures incorporating the optimized HfO_x are shown in Fig. 3. Very little hysteresis is observed in these curves. The fixed charge density is estimated to be 2.25×10^{12} cm^{-2} and the flat band voltage is -1.5 V. The dielectric constant of the HfO_x is

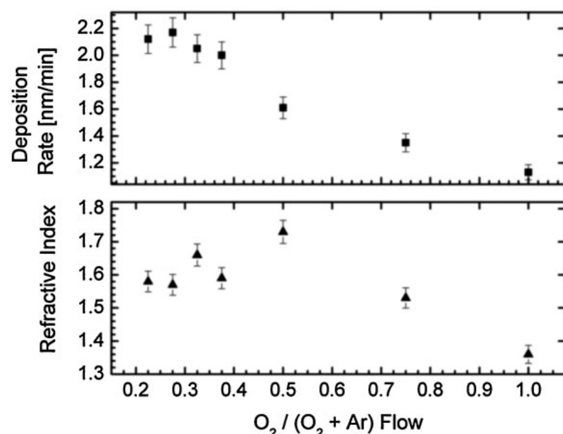

Figure 1 Variation in the deposition rate and refractive index of rf magnetron sputtered HfO_x samples as a function of O_2/Ar flow ratios.

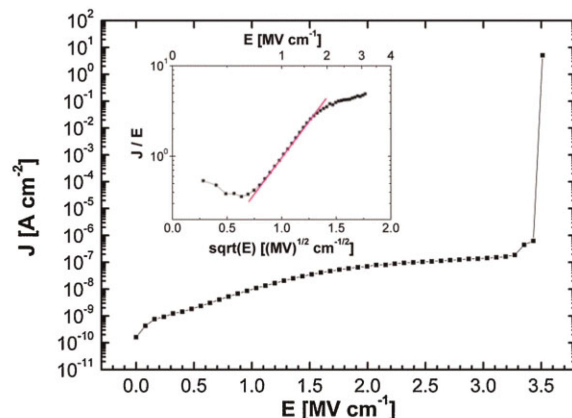

Figure 2 Leakage current density as a function of electric field for an optimized rf magnetron sputtered HfO_x dielectric film (~ 100 nm thick). Inset shows a Poole-Frenkel plot.

© 2013 WILEY-VCH Verlag GmbH & Co. KGaA, Weinheim

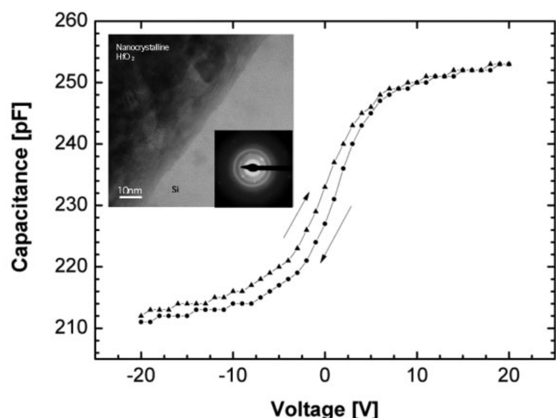

Figure 3 Capacitance–voltage characteristics for an optimized rf magnetron sputtered HfO_x dielectric film (~100 nm thick). Measurements were performed using MIS capacitor structures. Inset is a TEM micrograph of a typical film with associated electron diffraction pattern showing the presence of nanocrystals of HfO_x embedded in an amorphous matrix. The lattice spacing observed in the crystalline regions is consistent with a monoclinic structure.

found to be 18.2, which is comparable with measurements performed on material deposited by PLD and ALD [2, 44].

The microstructure of the optimized rf magnetron sputtered HfO_x has been investigated (inset to Fig. 3) by TEM. The results revealed that the material is nanocrystalline in nature with randomly oriented, small crystals ~10 nm in diameter being embedded within an amorphous matrix. This is consistent with the electron diffraction pattern which consists of broad, amorphous rings together with bright spots that are caused by the presence of the crystals (see inset to Fig. 3).

The fact that the crystals are very small and are surrounded by amorphous material means that there are no grain boundaries which extend through the whole thickness of the insulating layer. Consequently, the resistivity is high and relatively uniform across the sample. It is likely that the surface of the crystals is highly defective, and these may act as traps for electrons, which is consistent with the Poole-Frenkel tunnelling mechanism that dominates the conduction process.

3.2 HiTUS films The growth mechanism of thin films deposited by the HiTUS system is very different to that deposited by the rf magnetron sputtering system. In the latter case, oxidation takes place near the target, and the primary species sputtered from the target is likely to be HfO_x. In such a configuration, target poisoning (i.e., over-oxidation of the target) is a major concern. In contrast, for the HiTUS system, the oxygen gas is injected close to the sample where it is effectively gettered by the depositing metal, and so oxidation occurs at or close to the substrate. This has two important consequences: first, the plasma beam is dominated by a flux of argon ions which bombard the metallic hafnium target, and second, the absence of oxygen in the plasma means that there is no oxygen ion bombardment of the sample. For the purposes of depositing high quality HfO_x, it is therefore clearly critical that there is sufficient oxygen in the system relative to the metallic sputtering rate for full oxidation of the sample, but not excess oxygen so that oxygen starts to enter the sputtering plasma leading to both oxygen ion bombardment and target poisoning.

Therefore, initial development of HiTUS HfO_x thin films focused on examining the variation in material properties as a function of target power and oxygen flow rate, which largely controls the sputtering rate of metallic content and the oxidation rate of the metallic species, respectively. As shown in Fig. 4a, the deposition rate increases with target power (with all other parameters fixed), which can be explained by an increase in sputtering rate of the metal target. This increase in metallic content of the HfO_x thin film is reflected in the increase in the refractive index (due to increasing density [45]) with increase in target power in Fig. 4b, and in the decrease in the electrical resistivity as target power increases above 900 W in Fig. 4c. Excessive target power also causes a drop in the breakdown field, as shown in Fig. 4d, which is most likely due to a reduction in the insulating properties with increased metallic content. Figure 4e reveals an increase in the dielectric constant from 23 to 32 as the target power increases from 600 to 1200 W. Both the increase in refractive index and in dielectric constant suggests densification of the thin film with increasing target

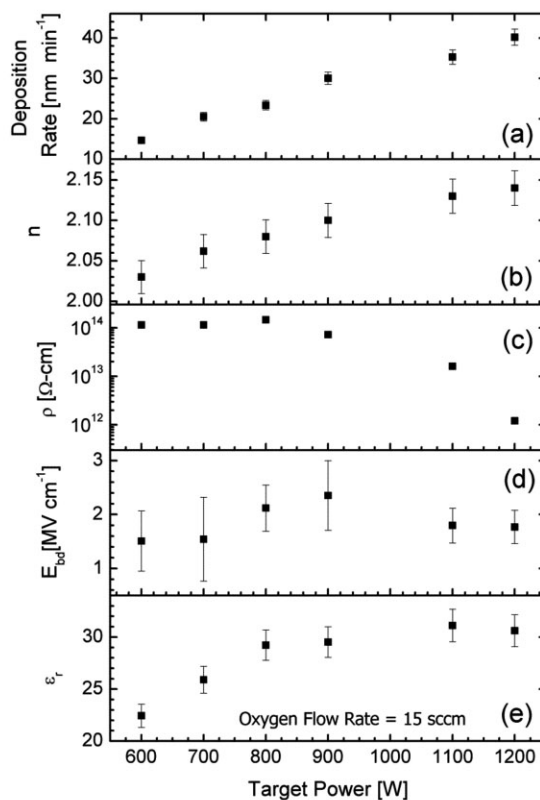

Figure 4 Variation in the (a) deposition rate, (b) refractive index, (c) resistivity, (d) breakdown field and (e) dielectric constant of HiTUS HfO_x as a function of target power.

© 2013 WILEY-VCH Verlag GmbH & Co. KGaA, Weinheim

power [45, 46]. In general, to be suitable as a gate dielectric in TFTs, we want to select a film with the highest resistivity and the highest breakdown strength. From this study of the impact of target power, it is concluded that, for the deposition conditions considered here (15 sccm of oxygen), a target power of 800–900 W appears optimal. This results in a deposition rate of $\sim$25 nm min^{-1}, an average refractive index of 2.09, an average resistivity of 10^{14} Ω cm, an average breakdown field of 2.5 MV cm^{-1} and a dielectric constant of 30.

The impact of oxygen flow rate on the deposition rate of HfO_x is illustrated in Fig. 5a. As the oxygen flow rate increases, the deposition rate decreases as a result of increased oxidation at the target surface. When the oxygen flow rate is too low, there is insufficient oxidation near the substrate and sputtering of metal atoms dominates the deposition process to yield a higher deposition rate. However, this leads to HfO_x films with a relatively high refractive index and an undesirably low resistivity as shown in Fig. 5b and c, respectively, suggesting too much metallic content. On the other hand, when the oxygen flow rate is sufficiently high, the oxidation process dominates over the sputtering process, leading to a more resistive film deposited at a lower rate. A high oxygen flow rate is necessary to trigger sufficient oxidation to yield HfO_x films with a higher breakdown field (see Fig. 5d). To be applicable as a gate dielectric material, HfO_x needs to be as resistive as possible with a high breakdown strength. Thus, a high oxygen flow rate is desirable, but at the expense of a lower deposition rate. The importance of an adequate quantity of oxygen species in metal oxides is key as oxygen vacancies are normally the dominant source of charge traps in HfO_x films. It has been reported that deposition and/or post-processing conditioning in an oxygen-rich ambient is desirable for removal or passivation of these defects [47]. Thus, it appears that a high oxygen flow rate is required for reducing the defect density in HfO_x. Figure 5e reveals a decrease in the dielectric constant from 34 to 24 as the oxygen flow rate increases from 12 to 20 sccm. The concurrent decrease in refractive index and in dielectric constant suggests a reduction in the film density with oxygen flow rate, which can be explained by a reduction in the relative metallic content in the film [45]. From this study of the impact of the oxygen flow rate, it is concluded that, for the deposition conditions considered here (800 W of target power), an oxygen flow rate of 14–15 sccm appears optimal, resulting in a deposition rate of $\sim$25 nm min^{-1}, an average refractive index of 2.1, an average resistivity of 10^{14} Ω cm, an average breakdown field of $\sim$3 MV cm^{-1} and a dielectric constant of up to $\sim$32.

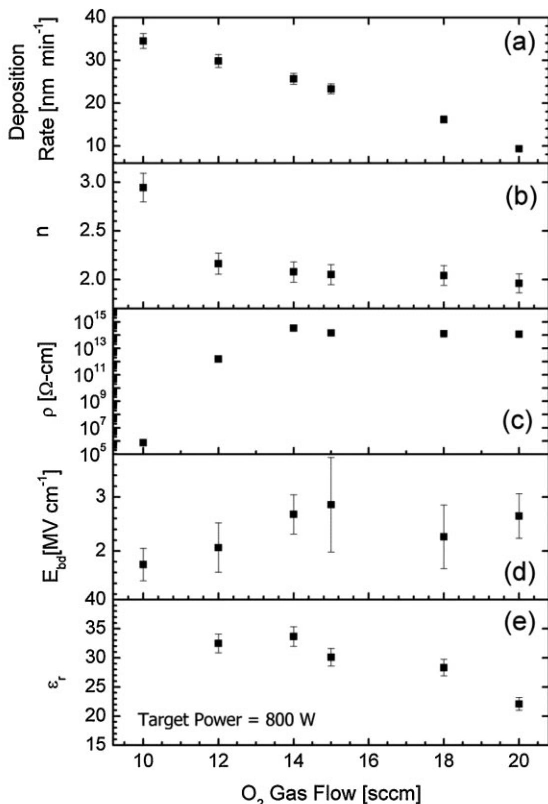

Figure 5 Variation in the (a) deposition rate, (b) refractive index, (c) resistivity, (d) breakdown field, and (e) dielectric constant of HiTUS HfO_x as a function of oxygen flow rate.

Figure 6 (adapted from the authors' previous report on this material [38]) plots the leakage current density as a function of electric field for an "optimized" HfO_x thin film (deposited at target power of 800 W and oxygen flow rate of 15 sccm). A leakage current density in the range of 1–10 nA cm^{-2} is observed for electric fields <1 MV cm^{-1}. Under moderately high electric fields ($\sim$1.5–2 MV cm^{-1}), Schottky Emission conduction dominates, as can be seen by the linear form of the graph shown as the inset to Fig. 6. In these conditions, the barrier ϕ_b between the Fermi energy in a metal and the conduction band in an insulator is sufficiently lowered to allow thermally excited carriers to make this

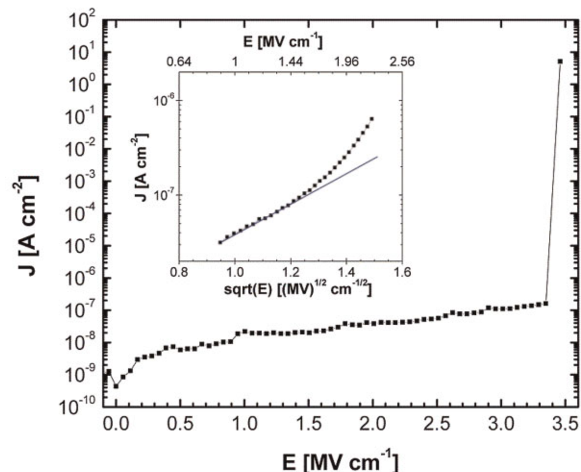

Figure 6 Leakage current density as a function of electric field characteristics for an optimized HiTUS HfO_x thin film (adapted from Ref. [38]). The film thickness is approximately 100 nm. Inset shows a Schottky Emission plot in the high field regime. Measurements were performed using an MIS capacitor structure.

© 2013 WILEY-VCH Verlag GmbH & Co. KGaA, Weinheim

transition, resulting in a Schottky Emission Current, which is described by

$$J = cT^2 \exp\left(\frac{a\sqrt{E} - b\phi_b}{k_B T}\right) \quad (3)$$

where J is the current density, E the electric field strength, ϕ_b the barrier height, k_B the Boltzmann constant, T the absolute temperature, and a, b, and c are constants. In comparison to the trap-assisted Poole-Frenkel conduction observed in rf magnetron sputtered HfO_x films, the observation of Schottky emission for HiTUS sputtered HfO_x is an indication of an apparent reduction in the bulk defect density in the film. Schottky emission has also been reported in rf sputtered HfO_2 after annealing at 500 °C in a N_2 atmosphere [48], and in PLD HfO_2 annealed at 500 °C in N_2 [49]. By comparison, an advantage of HiTUS HfO_x is the ability to obtain equivalently good quality films (controlled defect density) without substrate heating during growth or post-deposition annealing. Temperature-dependent current–voltage measurements are being examined to develop a better understanding of the underlying current conduction mechanisms.

The capacitance–voltage curves for the MIS structures incorporating the "optimized" HfO_x have been previously reported by the authors [38]. The dielectric constant of this HfO_x is found to be 30.6. Very little hysteresis is observed; the fixed charge density is estimated to be $3.76 \times 10^{12}\,cm^{-2}$ and the flat band voltage is 2.5 V.

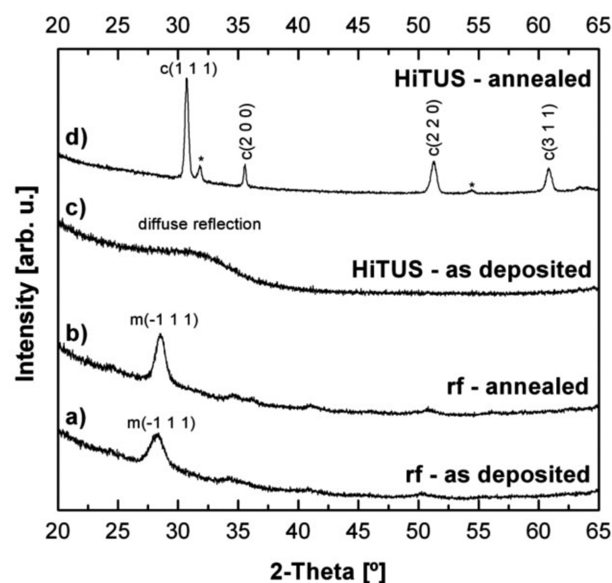

Figure 7 X-ray diffraction (XRD) scans of typical as-deposited (a) and vacuum annealed (b) rf-magnetron sputtered HfO_x films as well as as-deposited (c) and vacuum annealed (d) HiTUS HfO_x films. The labeled peak in (a) and (b) can be assigned to the strongest reflection of monoclinic HfO_2 (labelled m, ICDD-PDF file 34-0104). The broad diffraction feature around ~32° in (c) is ascribed to amorphous HfO_x, while (d) matches the diffraction pattern of polycrystalline cubic HfO_2 (labelled c, ICDD-PDF file 53–0550; * Designates two reflections from a minor contribution from another phase that is ambiguous to assign).

The microstructure of typical HiTUS HfO_x samples has been studied by XRD and compared to typical rf-magnetron sputtered films in Fig. 7. To seek more in-depth insights in the film microstructure, we also examined the XRD scans of rf magnetron sputtered and HiTUS films after vacuum annealing (~10^{-7} mbar) at ~640 °C for 35 min. The as-deposited rf magnetron sputtered film shows a diffraction peak corresponding to the most intense reflection of monoclinic HfO_2 (Fig. 7a). This is commonly assigned to monoclinic nanocrystallites [50] and is in agreement with our TEM results (Fig. 3inset). The XRD scan for the rf magnetron sputtered film does not change significantly after annealing (Fig. 7b), indicating the film does not undergo further crystallization.

In contrast, the as-deposited HiTUS HfO_x film exhibits only a very diffuse reflection centered around 32° (Fig. 7c) which is commonly ascribed to an amorphous structure [51], which, by definition, refers to a solid with no long-range order but with local short-range order of 1–2 bond lengths distance. We have previously confirmed the amorphous structure of these HiTUS films by TEM (see Fig. 3 in Ref. [38]).

The annealed HiTUS film exhibits a clear diffraction pattern of predominantly polycrystalline cubic HfO_2 (with a small contribution of another ambiguous phase), as shown in Fig. 7d. The crystallographic evolution from an amorphous to a predominantly cubic phase is rare for HfO_2 films, as the appearance of a cubic phase is commonly accompanied by other polymorphs [52, 53]. Based on this unusual crystallization behavior we suggest that the as-deposited amorphous HiTUS HfO_x possesses a disordered cubic-like short-range order (i.e., the Hf atoms tend to be eightfold coordinated and the O atoms tend to be fourfold coordinated as opposed to the monoclinic coordination of seven for Hf and either three or four for O) [54]. This short-range order acts as nucleation sites for topotactic rearrangement to yield a crystalline cubic phase upon high temperature annealing.

This is consistent with the high k of 30 measured in HiTUS films, since k values in the range of 30–35 are often linked to cubic polymorphs of HfO_2 [36, 37]. Such a connection between a high k in amorphous HfO_2 and a cubic-like short-range order was also suggested by recent simulations of the structure and dielectric properties of amorphous HfO_x [55]. This cubic-like amorphous hafnium oxide (ca-HfO_x) is in contrast to the rf magnetron sputtered HfO_x, which is monoclinic and possesses a significantly lower $k \sim 18$. This is in good agreement with previously published literature where the monoclinic phase (incl. monoclinic-like local coordination in amorphous films) is often linked to a lower k value ($k \sim 20$) [36, 37, 56].

Further characterization shows that the HiTUS ca-HfO_x has an optical (Tauc) gap of ~5.4 eV. Depth resolved XPS measurements demonstrate only signals from Hf and O in the films (not shown) and thus establish that the HiTUS films are free from any elemental impurities. This is important

© 2013 WILEY-VCH Verlag GmbH & Co. KGaA, Weinheim

Table 1 Summary of physical properties of rf magnetron sputtered HfO_x and HiTUS *ca*-HfO_x thin films. Properties of high quality rf-PECVD silicon nitride dielectric (from Ref. [59]) are also included for comparison. The values quoted for HfO_x correspond to the "optimized" recipes.

parameter	rf magnetron sputtered HfO_x	HiTUS *ca*-HfO_x	rf-PECVD silicon nitride
substrate temperature (°C)	25	25	300
deposition rate (nm min^{-1})	1.6	25	6.2
refractive index	1.73	2.05	1.9
resistivity (Ω cm) at 1 MV cm^{-1}	3.8×10^{13}	1.4×10^{14}	1×10^{14}
breakdown field (MV cm^{-1})	3.5	3	10
dielectric constant	18.2	30	7.5
structure	nano-crystalline	amorphous	amorphous
"optimized" recipe	1:1 O_2:Ar flow ratio	15 sccm O_2 flow, 800 W target power	see Ref. [59]

since impurities have previously been reported to stabilize metastable HfO_2 polymorphs [30, 57, 58], and thus the purity of the samples (XPS sensitivity limit <0.1–1%) ensures that the unique film properties are only related to the HiTUS deposition. A Hf:O stoichiometry ratio of 1:2.1 is estimated from XPS.

The HiTUS films exhibit an average resistivity of 1.2×10^{14} Ω cm and a breakdown strength in excess of 3 MV cm^{-1}. These properties are comparable to those of PECVD silicon nitride for a-Si:H TFTs (see Table 1) [59] and fulfill the requirements for such a gate dielectric material.

Based on the XRD results, it is observed that the HiTUS deposition system can produce *ca*-HfO_x without intentional substrate heating (heating from momentum transfer and secondary electrons is significantly less than 100 °C). Crystallization during room temperature magnetron sputter deposition can be attributed to bombardment of the sample surface by oxygen ions [46, 60]. As discussed previously, such oxygen ions are not normally present in HiTUS sputtering, allowing the direct formation of an amorphous material.

However, there is a second issue as to the reason why the HiTUS deposition permits the formation of a cubic-like short-range order while rf magnetron sputtering favors monoclinic structures. In general, the monoclinic phase of hafnium oxide is favored at room temperature and pressure (RTP) as it has the lowest free energy of formation and the lowest density [1]. Therefore, it was expected that the amorphous state of this material would also favor a monoclinic short-range order [56]. However, it is known that other materials which can exist in a number of crystalline phases do not always adopt the short range order of the lowest free energy phase in their amorphous state at RTP.

Perhaps the most well-known of these is carbon. In this case, the graphitic phase has a lower free energy than the diamond phase, but under the correct growth conditions, amorphous thin films may be deposited with predominantly diamond-like (sp^3) short-range order rather than graphitic-like (sp^2) short-range order [61]. Diamond-like carbon (DLC) material with a high sp^3 content is frequently deposited by ion-assisted deposition techniques, such as filtered cathodic vacuum arc (FCVA) [62]. In these cases, the sp^3 content is highly dependent on the energy of the carbon species arriving at the growth surface, with the highest sp^3 content achieved for ion energies of ~100 eV [63]. This is explained by a subplantation model [61]. If the incoming carbon ion has an energy, E_i, that is less than a penetration threshold energy, E_p, then it will only be able to bind to the growth surface without penetration. In the absence of any constraints, the low energy sp^2 bonding results. However, if $E_i > E_p$, then the ion will penetrate below the surface, increasing the density in this subsurface growth zone, with the result that the ion takes up the more dense sp^3 bonding configuration. Provided that there is not a large quantity of excess energy to allow relaxation of the system back to the low energy sp^2 state, then a DLC material will result.

In this work, it is postulated that the HiTUS sputter conditions allow a similar subplantation process to occur, leading to the formation of *ca*-HfO_x, rather than a monoclinic-like amorphous material. The key material parameter in assessing this is E_p. This is not a simple parameter to assess as it is known that the surface of the *ca*-HfO_x is only partially oxidized at any moment in time during growth. For simplicity, the case of metallic Hf will be considered in the first instance. When an atom or ion arrives at the growing surface, there is an energy gain associated with surface binding, E_b, as the surface appears as an attractive potential. Therefore, the total energy of the incoming atom or ion is $E_i + E_b$. This surface binding energy is 6.85 eV for Hf [64]. For penetration to occur, the total energy of the incoming atom, $E_i + E_b$, must exceed the displacement threshold energy E_d, so

$$E_p = E_d - E_b. \quad (4)$$

There are no reports of the value of E_d value for Hf, but it is known empirically that E_d is between four and five times greater than the cohesive energy for most metals [65], and so 29 eV would be a good estimation, suggesting a penetration energy of ~24 eV. Therefore, for the higher density *ca*-HfO_x to be formed, the Hf atoms arriving at the growth surface must have an energy greater than this, otherwise a monoclinic microstructure will result.

© 2013 WILEY-VCH Verlag GmbH & Co. KGaA, Weinheim

Using the work of Drüsedau et al. [66], it is possible to estimate both the average and maximum energies, $\langle E_{at}\rangle$ and E_{max}, respectively, of incoming Hf atoms from rf magnetron and HiTUS sputtering. E_{max} is given by

$$E_{max} = \kappa\Gamma E_0 - E_b, \quad (5)$$

where κ is the energy dissipation in the collision cascade (0.42 for Hf from Ref. [66]), Γ is the sputtering efficiency, which is 0.60 for Hf sputtering with Ar ions and E_0 is the energy of the incoming Ar ions. The average kinetic energy is then given by

$$\langle E_{at}\rangle = E_b^{2/3} E_{max}^{1/3}. \quad (6)$$

Therefore, given that for both rf magnetron sputtering and HiTUS sputtering, low pressure regimes are employed with low probabilities of gas phase interactions between the target and sample, E_0 is the key parameter controlling the energetics of the arriving Hf species which is different between the two systems. For the rf magnetron sputtering system, E_0 will be limited to the dc offset potential of the target, which is measured to be ~145 V. Substituting 145 eV for E_0 into Eq. (5) gives 36.5 eV for E_{max} and hence 12.0 eV for $\langle E_{at}\rangle$. Hence, very few species are likely to have an energy greater than E_p. In the case of HiTUS deposition, however, E_0 is very well defined by the target potential, which is measured to be 520 eV. This results in significantly higher values for both E_{max} and $\langle E_{at}\rangle$ of 124 and 18 eV, respectively. In this case, a significant proportion of the depositing Hf species will have sufficient energy to subplant below the growing surface, leading to material densification, and the formation of the cubic-like short range order, as observed experimentally, and illustrated in Fig. 8.

The proposed mechanism for ion bombardment induced growth of cubic-like amorphous (short-range ordered) hafnium oxide at low temperature using the HiTUS process, as described above, is simplistic in that it does not account for (i) variable collision angle incident on complex bonds and unbound species present within the lower density evolving growth front and (ii) associated collision cascade events as they penetrate into the altered layer (densifying transition thickness) with concomitant atomic movement that promotes the formation of the bulk cubic-like amorphous oxide film properties observed.

The specific nature and properties of the bombarding species, the importance of the atom-to-ion arrival rate ratio and energy range, and the role played by the chemisorbed oxygen at the onset of the coating growth need further investigation in order to develop a better understanding of the mechanism(s) by which the ion bombardment, as provided by the HiTUS process, imparts a window of energy to promote appropriate molecular dissociation, lattice displacement, and atomic rearrangement under minimal damage and stress relaxation conditions that are believed to be at the heart of the low temperature production of *ca*-HfO_x.

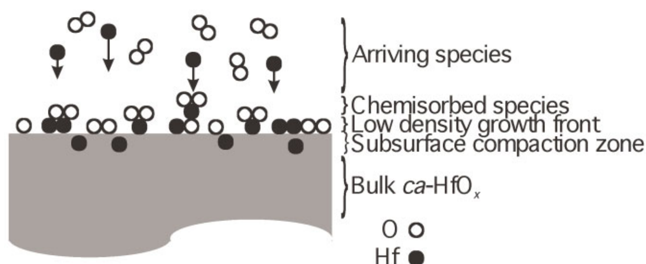

Figure 8 Schematic illustration of the growth of *ca*-HfO_x using the HiTUS process highlighting the presence of well-defined growth zones. The top surface is dominated by chemisorbed species (most notably molecular oxygen). Beneath this there is a low-density growth front due to deposition by low energy presursors, with a further subsurface compaction zone below this where subplantation is occurring. Both the growth front and compaction zone are likely to be only a few monolayers think, and therefore chemisorbed oxygen will diffuse into this region.

3.3 Material comparison for large-area electronic applications Table 1 compares the properties of HfO_x thin films deposited at room temperature by rf magnetron sputtering with *ca*-HfO_x deposited by the HiTUS system and silicon nitride deposited at 300 °C by rf plasma enhanced chemical vapor deposition (rf-PECVD), as used in a-Si:H TFTs. Generically, it is clear that the resistivity and breakdown strength of the HfO_x material deposited by either technique is of the same order as for silicon nitride, and this makes the application of HfO_x as the gate dielectric in TFTs viable. However, there is the advantage that the dielectric constant of the *ca*-HfO_x is significantly higher than for silicon nitride, which allows a greater on-state current for the same applied gate voltage, and the deposition temperature is compatible with the use of plastic substrates. This will be of particular relevance in TFTs for AMOLED displays.

However, the HiTUS *ca*-HfO_x has further key advantages over the rf sputtered material. The elimination of oxygen ion bombardment in the HiTUS system means that material can be deposited with an amorphous microstructure. This has a profound influence upon electrical properties as conduction under the application of moderate fields is now dominated by surface effects (Schottky emission) rather than bulk defects associated with grain boundaries (Poole-Frenkel tunneling). It is for this reason that the HiTUS *ca*-HfO_x has a significantly enhanced resistivity and dielectric constant compared with rf magnetron sputtered HfO_x. The HiTUS material is also more dense, as can be seen by comparing both the refractive index and dielectric constant (see Table 1) [45, 46]. Also, from a manufacturability perspective, the significantly higher growth rate achieved by HiTUS sputtering makes this technique intrinsically more cost effective for large-area electronics.

4 Conclusions It has been demonstrated that high-k amorphous HfO_x dielectric layers can be grown without substrate heating by the HiTUS system from a metallic hafnium target. The thin films produced using the HiTUS process demonstrate a high resistivity of up to $10^{14}\,\Omega\,$cm,

 © 2013 WILEY-VCH Verlag GmbH & Co. KGaA, Weinheim

high breakdown strength of 3 MV cm^{-1}, and a high dielectric constant of 30. These properties are superior to rf magnetron sputtered HfO_x thin films, which are characterized by a lower electrical resistivity, a lower dielectric constant, a higher defect density and a nanocrystalline microstructure. The amorphous phase is facilitated in the HiTUS process by the absence of oxygen ion bombardment of the substrate during growth. The amorphous HfO_x produced by the HiTUS system is characterized by a much higher k and formed at a higher deposition rate than other previously reported amorphous HfO_2 films. XRD results of HiTUS HfO_x indicate that the film possesses a short-range order dominated by cubic-like atomic coordination which leads to the high k values measured. It is postulated that the HiTUS process allows growth of this cubic-like amorphous (*ca*-)HfO_x material through a higher energy of depositing Hf species compared with rf magnetron sputtering, which exceeds the threshold penetration energy leading to material densification through subplantation. The *ca*-HfO_x produced is compatible with use as the gate dielectric layer in TFTs for AMOLED displays on plastic substrates, and is an attractive dielectric option for other large-area electronic applications.

Acknowledgements The authors acknowledge the financial support of this project provided by the Centre for Advanced Photonics and Electronics (CAPE) through the HiMo Project, by the EPSRC through the Cambridge Integrated Knowledge Centre's HiPZOT Project (grant no. EP/E023614/1) and the FlexIC Project (grant no. TS/I001158/1), and by the European Communities Seventh Framework Programme "ORAMA" project (grant agreement CP-IP 246334-2).

References

[1] J. H. Choi, Y. Mao, and J. P. Chang, Mater. Sci. Eng. R **72**, 97 (2011).
[2] Y.-S. Lin, R. Puthenkovilakam, and J. P. Chang, Appl. Phys. Lett. **81**, 2041 (2002).
[3] P. W. Peacock and J. Robertson, J. Appl. Phys. **92**, 4712 (2002).
[4] J. Robertson, Eur. Phys. J. Appl. Phys. **28**, 265 (2004).
[5] J. Robertson, J. Appl. Phys. **104**, 124111 (2008).
[6] R. Kanjolia, Semicond. Int. **30**, 32 (2007).
[7] D. Scansen, Electron. Eng. Times **1532** (Suppl), 58 (2008).
[8] P. F. Carcia, R. S. McLean, and M. H. Reilly, Appl. Phys. Lett. **88**, 123509 (2006).
[9] E. Fortunato, A. Pimentel, L. Pereira, A. Goncalves, G. Lavareda, H. Aguas, I. Ferreira, C. N. Carvalho, and R. Martins, J. Non-Cryst. Solids **338–340**, 806 (2004).
[10] E. M. C. Fortunato, P. M. C. Barquinha, A. Pimentel, A. M. F. Goncalves, A. J. S. Marques, R. F. P. Martins, and L. M. N. Pereira, Appl. Phys. Lett. **85**, 2541 (2004).
[11] R. L. Hoffman, B. J. Norris, and J. F. Wager, Appl. Phys. Lett. **82**, 733 (2003).
[12] D. H. Levy, D. Freeman, S. F. Nelson, P. J. Cowdery-Corvan, and L. M. Irving, Appl. Phys. Lett. **92**, 192101 (2008).
[13] S.-H. K. Park, C.-S. Hwang, M. Ryu, S. Yang, C. Byun, J. Shin, J.-I. Lee, K. Lee, M. S. Oh, and S. Im, Adv. Mater. **21**, 678 (2009).
[14] P. F. Carcia, R. S. McLean, M. H. Reilly, M. K. Crawford, E. N. Blanchard, A. Z. Kattamis, and S. Wagner, J. Appl. Phys. **102**, 074512 (2007).
[15] P. Barquinha, G. Gonçalves, L. Pereira, R. Martins, and E. Fortunato, Thin Solid Films **515**, 8450 (2007).
[16] D. C. Paine, B. Yaglioglu, Z. Beiley, and S. Lee, Thin Solid Films **516**, 5894 (2008).
[17] E. Fortunato, N. Correia, P. Barquinha, L. Pereira, G. Goncalves, and R. Martins, IEEE Electron Device Lett. **29**, 988 (2008).
[18] K. Nomura, H. Ohta, A. Takagi, T. Kamiya, M. Hirano, and H. Hosono, Nature **432**, 488 (2004).
[19] H. Yabuta, M. Sano, K. Abe, T. Aiba, T. Den, H. Kumomi, K. Nomura, T. Kamiya, and H. Hosono, Appl. Phys. Lett. **89**, 112123 (2006).
[20] D. E. Mentley, Proc. IEEE **90**, 453 (2002).
[21] R. A. Street, Hydrogenated Amorphous Silicon (Cambridge University Press, Cambridge, 1991).
[22] A. J. Flewitt and W. I. Milne, Proc. IEEE **93**, 1364 (2005).
[23] K. R. Sarma, C. Chanley, S. Dodd, J. Roush, J. Schmidt, G. Srdanov, M. Stevenson, R. Wessel, J. Innocenzo, G. Yu, M. O'Regan, W. A. MacDonald, R. Eveson, K. Long, H. Gleskova, S. Wagner, and J. C. Sturm, Proc. SPIE **5080**, 180 (2003).
[24] A. Sazonov, A. Nathan, and D. Striakhilev, J. Non-Cryst. Solids **266–269**, 1329 (2000).
[25] B. Stannowski, R. E. I. Schropp, R. B. Wehrspohn, and M. J. Powell, J. Non-Cryst. Solids **299**, 1340 (2002).
[26] C.-S. Yang, L. Smith, C. Arthur, and G. Parsons, J. Vac. Sci. Technol. B **18**, 683 (2000).
[27] J.-C. Goh, J. Jang, K.-S. Cho, and C.-K. Kim, IEEE Electron Device Lett. **24**, 583 (2003).
[28] K. Sakariya, P. Servati, and A. Nathan, IEEE Trans. Electron Devices **51**, 2019 (2004).
[29] K. Nomura, H. Ohta, H. A. Masahiro, K. Ueda, T. Kamiya, M. Hirano, and H. Hosono, Microelectron. Eng. **72**, 294 (2004).
[30] T. Wang and J. G. Ekerdt, Chem. Mater. **21**, 3096 (2009).
[31] H. Gruger, C. Kunath, E. Kurth, S. Sorge, W. Pufe, and T. Pechstein, Thin Solid Films **447–448**, 509 (2004).
[32] L. Pereira, P. Barquinha, E. Fortunato, and R. Martins, Mater. Sci. Eng. B **118**, 210 (2005).
[33] R. Jiang, E. Q. Xie, and Z. F. Wang, Appl. Phys. Lett. **89**, 142907 (2006).
[34] C.-H. Lu, Y.-S. Lai, and J. S. Chen, J. Electrochem. Soc. **153**, F189 (2006).
[35] J. E. Jaffe, R. A. Bachorz, and M. Gutowski, Phys. Rev. B **72**, 144107 (2005).
[36] X. Zhao and D. Vanderbilt, Phys. Rev. B **65**, 233106 (2002).
[37] G. M. Rignanese, X. Gonze, G. Jun, K. Cho, and A. Pasquarello, Phys. Rev. B **69**, 184301 (2004).
[38] F. M. Li, B. C. Bayer, S. Hofmann, J. D. Dutson, S. J. Wakeham, M. J. Thwaites, W. I. Milne, and A. J. Flewitt, Appl. Phys. Lett. **98**, 252903.1 (2011).
[39] A. J. Flewitt, J. D. Dutson, P. Beecher, D. Paul, S. J. Wakeham, M. E. Vickers, C. Ducati, S. P. Speakman, W. I. Milne, and M. J. Thwaites, Semicond. Sci. Technol. **24**, 085002.1 (2009).
[40] W. D. Sproul, D. J. Christie, and D. C. Carter, Thin Solid Films **491**, 1 (2005).
[41] A. J. Flewitt, A. P. Dyson, J. Robertson, and W. I. Milne, Thin Solid Films **383**, 172 (2001).
[42] D. R. Lide, Handbook of Chemistry and Physics, 86th ed. (CRC Press, Boca Raton, FL, 2005).

© 2013 WILEY-VCH Verlag GmbH & Co. KGaA, Weinheim

[43] S. M. Sze, Physics of Semiconductor Devices (Wiley, New York, 1981).
[44] K. Nomura, H. Ohta, K. Ueda, T. Kamiya, M. Hirano, and H. Hosono, Science **300**, 1269 (2003).
[45] M. Jerman, Z. Qiao, and D. Mergel, Appl. Opt. **44**, 3006 (2005).
[46] F. L. Martinez, M. Toledano-Luque, J. J. Gandia, J. Carabe, W. Bohne, J. Rohrich, E. Strub, and I. Martil, J. Phys. D, Appl. Phys. **40**, 5256 (2007).
[47] K. Xiong and J. Robertson, Microelectron. Eng. **80**, 408 (2005).
[48] H. W. Chen, F. C. Chiu, C. H. Liu, S. Y. Chen, H. S. Huang, P. C. Juan, and H. L. Hwang, Appl. Surf. Sci. **254**, 6112 (2008).
[49] H. Wang, Y. Wang, J. Zhang, C. Ye, H. B. Wang, J. Feng, B. Y. Wang, Q. Li, and Y. Jiang, Appl. Phys. Lett. **93**, 202904 (2008).
[50] E. E. Hoppe, R. S. Sorbello, and C. R. Aita, J. Appl. Phys. **101**, 123534 (2007).
[51] M. Modreanu, J. Sancho-Parramon, D. O'Connell, J. Justice, O. Durand, and B. Servet, Mater. Sci. Eng. B **118**, 127 (2005).
[52] M. Modreanu, J. Sancho-Parramon, O. Durand, B. Servet, M. Stchakovsky, C. Eypert, C. Naudin, A. Knowles, F. Bridou, and M. F. Ravet, Appl. Surf. Sci. **253**, 328 (2006).
[53] S. Miyake, I. Shimizu, R. R. Manory, T. Mori, and G. Kimmel, Surf. Coat. Technol. **146–147**, 237 (2001).
[54] G. H. Chen, Z. F. Hou, and X. G. Gong, Comput. Mater. Sci. **44**, 46 (2008).
[55] Y. Wang, F. Zahid, J. Wang, and H. Guo, Phys. Rev. B **85**, 224110 (2012).
[56] D. Ceresoli and D. Vanderbilt, Phys. Rev. B **74**, 125108 (2006).
[57] C. Dubourdieu, E. Rauwel, H. Roussel, F. Ducroquet, B. Hollander, M. Rossell, G. V. Tendeloo, S. Lhostis, and S. Rushworth, J. Vac. Sci. Technol. A **27**, 503 (2009).
[58] D. H. Triyoso, R. I. Hegde, J. K. Schaeffer, D. Roan, P. J. Tobin, S. B. Samavedam, B. E. White, Jr., R. Gregory, and X. D. Wang, Appl. Phys. Lett. **88**, 222901 (2006).
[59] A. J. Flewitt and W. I. Milne, in: Thin Film Transistors – Materials and Processes, Volume 1: Amorphous Silicon Thin Film Transistors, edited by Y. Kuo (Kluwer Academic, Massachusetts, 2004), Vol. 1, pp. 15.
[60] G. Reisse, S. Weissmantel, B. Keiper, B. Steiger, H. Johansen, T. Martini, and R. Scholz, Appl. Surf. Sci. **86**, 107 (1995).
[61] J. Robertson, Mater. Sci. Eng. R **37**, 129 (2002).
[62] P. Fallon, V. Veerasamy, C. Davis, J. Robertson, G. Amaratunga, W. Milne, and J. Koskinen, Phys. Rev. B **48**, 4777 (1993).
[63] M. Chhowalla, J. Robertson, C. W. Chen, S. R. P. Silva, C. A. Davis, G. A. J. Amaratunga, and W. I. Milne, J. Appl. Phys. **81**, 139 (1997).
[64] J. Emsley, The Elements (Clarendon Press, Oxford, UK, 1998).
[65] M. Nastasi, J. W. Mayer, and J. K. Hirvonen, Ion–Solid Interactions: Fundamentals Applications (Cambridge University Press, Cambridge, UK, 1996).
[66] T. P. Drüsedau, T. Bock, T.-M. John, F. Klabunde, and W. Eckstein, J. Vac. Sci. Technol. A **17**, 2896 (1999).

© 2013 WILEY-VCH Verlag GmbH & Co. KGaA, Weinheim